

SPH-simulation of shear induced powder migration in injection moulding

BY DAVID KAUZLARIĆ^{1,2}, LARS PASTEWKA³, HAGEN MEYER¹, RICHARD HELDELE⁴, MICHAEL SCHULZ⁴, OXANA WEBER⁴, VOLKER PIOTTER⁴, JÜRGEN HAUSSELT^{4,5}, ANDREAS GREINER¹, JAN G. KORVINK^{1,2}

¹*Laboratory for Simulation, Department of Microsystems Engineering, University of Freiburg, Georges-Köhler-Allee 103, 79110 Freiburg, Germany*

²*School of Soft Matter Research, Freiburg Institute for Advanced Studies, University of Freiburg, Albertstr. 19, 79104 Freiburg, Germany*

³*Fraunhofer Institute for Mechanics of Materials IWM, Wöhlerstr. 11, 79108 Freiburg, Germany*

⁴*Institute for Materials Research III, Karlsruhe Institute of Technology, Hermann-von-Helmholtz-Platz 1, 76344 Eggenstein-Leopoldshafen, Germany*

⁵*Laboratory for Materials Process Technology, Dept. of Microsystems Engineering, University of Freiburg, Georges-Köhler-Allee 102, 79110 Freiburg, Germany*

We present the application of the SPH-discretisation scheme to Phillips' model for shear induced particle migration in concentrated suspensions. This model provides an evolution equation for the scalar mean volume fraction of idealised spherical solid particles of equal diameter which is discretised by the SPH-formalism. In order to obtain a discrete evolution equation with exact conservation properties we treat in fact the occupied volume of the solid particles as the degree of freedom for the fluid particles. We present simulation results in 2D and 3D channel flow. The 2D results serve as a verification by a comparison to analytic solutions. The 3D results are used for a comparison with experimental measurements obtained from computer tomography of injection moulded ceramic micro-parts. We observe the best agreement of measurements with snapshots of the transient simulation for a ratio $D_c/D_\eta = 0.1$ of the two model parameters.

Keywords: SPH; concentrated suspensions; segregation; injection moulding

1. Introduction

A great need exists for micro-structured polymers, metals, and ceramics. The application areas range from DNA analysis instruments in life science over biocompatible materials for medical applications to a variety of electronic devices for sensors and actuators. Injection moulding [1] represents an economically efficient process for the micro-structuring of pure polymers or polymeric feedstocks with ceramic or metallic particle load. Micro powder injection moulding (MicroPIM) is a shaping process in which a highly filled polymer-powder compound (the feedstock) is heated above the melting temperature of the polymer and injected with pressure into a micro-cavity. The final ceramic or metallic micropart is obtained after subsequent debinding and sintering steps. To optimise part and mould design prior to tool construction and to reduce production costs there is a need for predictive process simulation.

There are a variety of finite element based simulation approaches [2, 3]. Usually, their disadvantage is the difficulty in handling free surfaces and large deformations. Similarly, commercial software tools are based on one-phase material models, *i.e.*, they show insufficient capabilities to simulate powder-binder mixtures. On the other hand, particle-based approaches are able to deal with free surfaces and large deformations easily. In this work we apply the method smoothed particle hydrodynamics SPH [4] to the simulation of the MicroPIM process. The simulation of casting with SPH was already successfully performed [5, 6]. Here, we have to apply this method to materials, which are rheologically more complex and which carry a solid load. In this work we focus on the shear induced segregation of the embedded powder particles [7-10], caused by the extremely high shear rates of up to 10^6 s^{-1} in MicroPIM. This may lead to non-homogeneous binder extraction during debinding or to an anisotropic shrinkage during sintering resulting in porosity, deformations or even cracks. Barriere et al. [3] accounted for segregation in a FE-simulation by implementing a two phase model. This paper presents a SPH-based approach describing the powder concentration as an internal degree of freedom.

After the presentation of the governing equations for fluid flow and of Phillips' model for shear induced particle migration [11] in section 2, we show their discretisation in section 3. Finally, we present several simulation results for the verification of the model, for the reproduction of experimental measurements, and for complex mould geometries in section 4.

2. Governing equations of motion

The basic equations used for the description of the MicroPIM-process are the continuity equation and the incompressible Navier-Stokes equation

$$\frac{d\rho}{dt} = -\rho \nabla \cdot \mathbf{v}, \quad \frac{d\mathbf{v}}{dt} = -\frac{\nabla P}{\rho} + \frac{1}{\rho} \nabla \cdot (\eta \nabla \mathbf{v}) \quad (2.1)$$

both given in a Lagrangian reference frame with mass density ρ , velocity \mathbf{v} , pressure P , and shear viscosity η . Segregation will be described by the diffusive flux model by Phillips *et. al.* [11]. This model is based on two diffusive fluxes \mathbf{J}_c and \mathbf{J}_η of a mean concentration of suspended particles ϕ . \mathbf{J}_c includes the migration mechanisms due to local variations in the collision frequency of the suspended particles and reads

$$\mathbf{J}_c = -D_c a^2 \phi \nabla(\phi \dot{\gamma}) = -D_c a^2 (\phi^2 \nabla \dot{\gamma} + \phi \dot{\gamma} \nabla \phi) \quad (2.2)$$

since variations in the collision frequency are caused by concentration gradients $\nabla \phi$ and variations in the shear rate $\nabla \dot{\gamma}$. The shear rate is defined in terms of the second invariant $\dot{\gamma} = \sqrt{\dot{\boldsymbol{\gamma}} : \dot{\boldsymbol{\gamma}}/2}$ of the strain rate tensor $\dot{\boldsymbol{\gamma}} = \nabla \mathbf{v} + (\nabla \mathbf{v})^T$. D_c is a diffusion constant and a is the particle diameter. D_c is an empirical parameter and has to be fitted by experiments. In addition a spatially varying viscosity due to a spatially varying particle concentration can lead to an effective particle flux as well. It reads

$$\mathbf{J}_\eta = -D_\eta \dot{\gamma} \phi^2 \left(\frac{a^2}{\eta} \right) \frac{\partial \eta}{\partial \phi} \nabla \phi \quad (2.3)$$

where D_η is an empirical dimensionless rate constant. Using both migration mechanisms the conservation equation for the volume fraction ϕ becomes

$$\frac{\partial \phi}{\partial t} = -\nabla \cdot (\phi \mathbf{v}) - \nabla \cdot (\mathbf{J}_c + \mathbf{J}_\eta) \quad (2.4)$$

The expression $\nabla \cdot \phi \mathbf{v}$ covers the convective transport of the suspended particles.

For the dependence of the viscosity on the volume fraction we assume the Krieger rheological model [12] which is

$$\eta(\phi) = \eta_0 \left(1 - \frac{\phi}{\phi_m}\right)^{-c}, \quad \frac{1}{\eta} \frac{\partial \eta}{\partial \phi} = \frac{c}{\phi_m - \phi}. \quad (2.5)$$

For a vanishing particle concentration the fluid has the reference viscosity η_0 and for the saturation volume fraction $\phi = \phi_m$ the viscosity diverges.

3. SPH discretisation

We briefly summarise the discretisation of fluid flow. For a detailed description of the SPH-discretisation formalism we refer the reader to the given references. We then show in detail how the diffusive flux model for powder migration is discretised.

To compute the evolution of the densities ρ_i of the SPH-particles indexed with i we discretise the equation of motion in (2.1), *i.e.*,

$$\dot{\rho}_i = \sum_j m_j \mathbf{v}_{ij} \cdot \nabla W_{ij} = - \sum_j m_j \mathbf{v}_{ij} \cdot \mathbf{r}_{ij} w_{ij} \quad (3.1)$$

where we have set $\mathbf{v}_{ij} = \mathbf{v}_i - \mathbf{v}_j$ and $\nabla W_{ij} = -\mathbf{r}_{ij} w_{ij}$. W_{ij} is the SPH-interpolation kernel and m_i a particle mass. This equation allows to simulate free surface flow [13]. The discretisation of the pressure gradient term in eq. (2.1) reads

$$\frac{(\nabla P)_i}{\rho_i} = \sum_j m_j \left(\frac{P_i}{\rho_i^2} + \frac{P_j}{\rho_j^2} \right) \nabla W_{ij}. \quad (3.2)$$

Incompressibility is approximated by a weakly compressible equation of state [13]

$$P(\rho) = P_0 \left[\left(\frac{\rho}{\rho_0} \right)^\gamma - 1 \right], \quad (3.3)$$

where $\gamma = 7$, ρ_0 is a reference density and $P_0 = c^2 \rho_0 / \gamma$, with the speed of sound c chosen large enough so that density fluctuations remain below 1%. The viscous term in the momentum equation in (2.1) is discretised as [14]

$$\left[\frac{1}{\rho} \nabla \cdot (\eta \nabla \mathbf{v}) \right]_i = - \sum_j m_j \frac{4\eta_i \eta_j}{\eta_i + \eta_j} \frac{w_{ij}}{\rho_i \rho_j} \mathbf{v}_{ij}. \quad (3.4)$$

Finally the tensor $\nabla \mathbf{v}$ can be discretised by [4]

$$(\nabla \mathbf{v})_i = \sum_j \frac{m_j}{\rho_j} \mathbf{v}_{ij} \nabla W_{ij} \quad (3.5)$$

which we require for the computation of the shear rate $\dot{\gamma}$ in eqs. (2.2) and (2.3).

Instead of discretising eq. (2.4) directly, it is better to use the equation of motion for the volume $V_\phi = \phi / \rho$ occupied by powder particles, where we have set the mass to $m = 1m^*$, *i.e.*, to the unit of mass m^* for simplicity. The discretised equation for

V_ϕ will be antisymmetric under exchange of fluid particles, leading to exact volume conservation. We have to switch from the Eulerian to the Lagrangian description. Introducing the material derivative $d/dt = \partial/\partial t + \mathbf{v} \cdot \nabla$ and substituting $\phi = \rho V_\phi$ gives

$$\frac{dV_\phi}{dt} = -V_\phi \frac{\dot{\rho}}{\rho} - V_\phi \nabla \cdot \mathbf{v} + \frac{1}{\rho} \nabla \cdot \left[D_c a^2 \phi \nabla(\phi \dot{\gamma}) + D_\eta \dot{\gamma} \phi^2 \frac{a^2}{\eta} \frac{d\eta}{d\phi} \nabla \phi \right] \quad (3.6)$$

which is the equation of motion for the occupied volume. The divergence of the velocity field gives the relative volume expansion, *i.e.*, $\nabla \cdot \mathbf{v} = \dot{V}/V = -\dot{\rho}/\rho$. Thus, the first two terms on the right hand side of (3.6) cancel. Now, we apply the rule for the SPH-discretisation of second derivatives [4]

$$(\nabla \cdot [B(\mathbf{r}) \nabla A(\mathbf{r})])_i \approx - \sum_j (B_i + B_j) (A_i - A_j) w_{ij} / \rho_j \quad (3.7)$$

for two scalar fields $A(\mathbf{r})$ and $B(\mathbf{r})$ to the right hand side of eq. (3.6). This is a simpler form than the discretisation (3.4) but we have not found any significant difference between the two forms for the results shown here. We get

$$\begin{aligned} \dot{V}_{\phi,i} = & -D_c a^2 \sum_j \frac{w_{ij}}{\rho_i \rho_j} (\phi_i + \phi_j) (\phi_i \dot{\gamma}_i - \phi_j \dot{\gamma}_j) \\ & - D_\eta a^2 \sum_j \frac{w_{ij}}{\rho_i \rho_j} \left(\dot{\gamma}_i \phi_i^2 \left(\frac{d\eta}{\eta d\phi} \right)_i + \dot{\gamma}_j \phi_j^2 \left(\frac{d\eta}{\eta d\phi} \right)_j \right) (\phi_i - \phi_j) \end{aligned} \quad (3.8)$$

Note that the expression within the sum is antisymmetric under particle exchange. In the discretised equation for $\dot{\phi}$, a factor $1/\rho_i$ is missing and the equation has no symmetry. The advantage of the antisymmetry is that volume is exactly conserved, because the amount of suspended volume that is deducted from particle i is added to particle j .

We finally have to consider the numerical implementation of the Krieger model. Both $\eta(\phi)$ and the derivative $(d\eta/d\phi)/\eta$ from eq. (2.5) diverge for $\phi \rightarrow \phi_m$. Therefore we have to use approximate expressions giving finite values for concentrations $\phi_c < \phi < \phi_m$, where ϕ_c is a critical limit. It is most convenient to start with an approximation for the relative derivative $(d\eta/d\phi)/\eta$. The lowest order approximation we can make is

$$\frac{1}{\eta_d} \frac{d\eta_d}{d\phi} = \begin{cases} \frac{1}{\eta} \frac{d\eta}{d\phi}, & \phi < \phi_c \\ \frac{1}{\eta} \frac{d\eta}{d\phi} \Big|_{\phi=\phi_c}, & \phi \geq \phi_c \end{cases} = \begin{cases} \frac{c}{\phi_m - \phi}, & \phi < \phi_c \\ \frac{c}{\phi_m - \phi_c}, & \phi \geq \phi_c \end{cases}, \quad (3.9)$$

where $\eta_d(\phi)$ represents the form of the Krieger model used for the discretised equations and may be obtained by solving the differential equation given in (3.9), *i.e.*,

$$\frac{d\eta_d}{d\phi} = \frac{c}{\phi_m - \phi_c} \eta_d(\phi), \quad \phi \geq \phi_c. \quad (3.10)$$

For a continuous transition to $\eta(\phi)$ at $\phi = \phi_c$ we need the boundary condition $\eta_d(\phi_c) = \eta(\phi_c)$. Then, solving (3.10) gives

$$\eta_d(\phi) = \begin{cases} \eta(\phi) = \eta_0 \left(1 - \frac{\phi}{\phi_m} \right)^{-c}, & \phi < \phi_c \\ \eta(\phi_c) \exp \left(c \frac{\phi - \phi_c}{\phi_m - \phi_c} \right), & \phi \geq \phi_c \end{cases}. \quad (3.11)$$

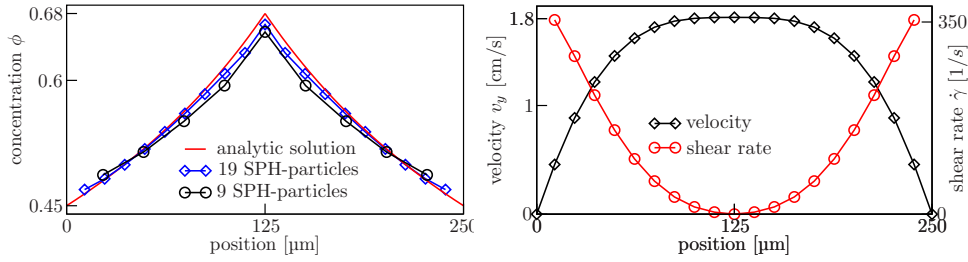


Figure 1. Left: Steady state analytic solution and computed powder concentration for Poiseuille flow for discretisations with 9 and 19 SPH-particles in the cross-section. Right: computed profiles of the flow velocity and the shear rate (second invariant). Symbols represent the values of the SPH-particles and lines serve for guiding the eye.

For $\phi = \phi_m$ a finite value $\eta_d(\phi_m) = \eta(\phi_c) e^c$ is obtained. Furthermore, since the approximation for the derivative (3.9) does not diverge for $\phi \rightarrow \phi_m$ the flux \mathbf{J}_η from eq. (2.3) is limited artificially and allows for particle concentrations $\phi > \phi_m$ above the packing limit. An unphysical effect is to be expected only when $\dot{\gamma} = 0$ and $\phi > \phi_c$. For the steady state simulations presented in this work it turns out that the smoothing effect of the SPH-discretisation (3.5) of $\dot{\gamma}$ counteracts and dominates over this approximation. In the transient simulations – which resemble the PIM-process more closely – the case $\phi > \phi_c$ never occurs.

4. Simulation results and discussion

The SPH-form of the Phillips-model is verified against an analytic solution by computing the concentration profile for pressure driven Poiseuille flow between two parallel plates. We choose $d_x = 250 \mu\text{m}$ as the width of the cross-section in x -direction. This width corresponds to the experimental setup for which measurements from computer tomography (CT) are available. The velocity component v_y is driven by a constant pressure gradient $p_y = 1.28 \text{ MPa/cm}$ which is implemented by applying an equivalent body-force on each SPH-particle in the periodic flow direction. The particle diameter is taken as $a = 0.01 \mu\text{m}$, $D_c = 1.17 \times 10^9$ is chosen such that the time constant for reaching steady state is as small as possible and we set $D_c/D_\eta = (1 + 1/c)^{-1} \approx 0.645$. This allows for an analytic solution of the steady state concentration profile which is for the left half of the channel $x' = [0, 1/2]$

$$\phi(x) = \frac{\phi_m \phi_0}{\phi_m - 2x'(\phi_m - \phi_0)} \quad (4.1)$$

with $x' \equiv x/d_x$ and where ϕ_0 is the concentration at the walls. Here we take $\phi_0 = 0.45$, $\phi_m = 0.68$ and $c = 1.82$ in accordance with Ref. [11].

The simulation is performed in 3D with periodic boundary conditions in the flow direction y and in z -direction. The cross-section in x -direction is discretised with two different resolutions of 9 and 19 SPH-particles which are initially at rest on a cubic lattice. The x -direction is confined by solid boundaries where no-slip boundary conditions are applied by boundary particles using the technique of Morris *et al.* [15]. By forbidding any exchange of ϕ between the SPH-particles representing the liquid and the SPH-particles representing the solid walls we assure zero migration across the boundaries. Fig. 1 shows the powder concentration, the velocity and the

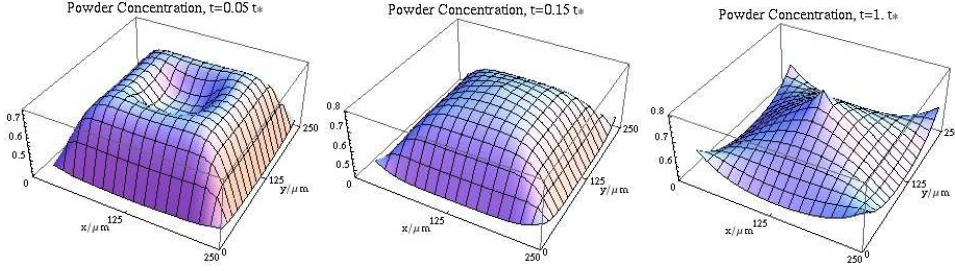


Figure 2. Transient evolution of the powder concentration to steady state as obtained from a simulation of flow through a quadratic $250 \mu\text{m} \times 250 \mu\text{m}$ channel cross-section.

shear rate profiles in steady-state and the analytic solution (4.1). One observes that the solid migrates to the centre of the channel and a blunted velocity profile. The latter is due to an increased viscosity in the centre because of the larger solids concentration. Hence, it is crucial to add the degree of freedom ϕ to account for its effect on the rheology. The computed concentration does not fully reach the analytic result $\phi = \phi_m = 0.68$ at the peak due to the smoothing of SPH. Thus, mass conservation leads to concentrations at the walls larger than $\phi_0 = 0.45$ as compared to the analytic solution. The error decreases when increasing the resolution.

Fig. 2 shows the transient evolution of the powder concentration as obtained from a simulation of flow through a quadratic $250 \mu\text{m} \times 250 \mu\text{m}$ channel cross-section. The simulation settings are the same as before except for $D_c/D_\eta = 0.4$, $a = 9 \mu\text{m}$, $\eta_0 = 33.2 \text{ Pas}$, $\phi_m = 0.794$ and $c = 0.714$ which are taken now from viscosity measurements of our feedstock “GoMicro” [9]. This corresponds to a “mean” viscosity $\eta(\bar{\phi}) = 100 \text{ Pas}$, where $\bar{\phi} = 0.625$. We have simulated different ratios D_c/D_η and have found that $D_c/D_\eta = 0.1$ reproduces best our computer tomography (CT) measurement for a specially prepared injection-moulded test-specimen [7, 9]. For this case, fig. 3 plots the concentrations at the centre line of the cross-section and also shows a concentration profile as obtained from CT and, for comparison, a profile obtained from a simulation with $D_c/D_\eta = 0.2$, showing the trend when increasing D_c/D_η . The right figure shows the CT-data in 2D. The global average concentration was conserved exactly in the simulations. In the simulations presented here, the equilibration of ϕ was boosted by purpose by choosing large constants D_c and D_η . Segregation starts close to the walls and propagates towards the centre where, after $t = 0.1 t^*$ a cusp starts to grow. Around this time the profile is similar with to our CT-measurement. This indicates that steady state was not reached during the MicroPIM process, *i.e.*, the longer the channel, the larger the segregation. Observe also the similarity between the central plot in fig. 2 and the right plot in fig. 3. It is known that the ratio of diffusion constants D_c/D_η is material dependent. Our value of $D_c/D_\eta = 0.1$ is small with respect to the physically reasonable range $[0..1]$ [11]. Hence, the flux \mathbf{J}_η from eq. (2.3) is dominant, which is a reasonable observation for highly viscous PIM-feedstocks.

As a more complex application of the powder migration model we consider the simulation of injection moulding into a 3D geometry. Some of our real PIM-parts are shown in fig. 4 a) and a snapshot of the filling simulation in b). The arrows in b) and d) indicate the flow direction at the gate. Besides the similarity of the flow patterns, a) and b) illustrate the advantages of SPH over FE-methods. The SPH-

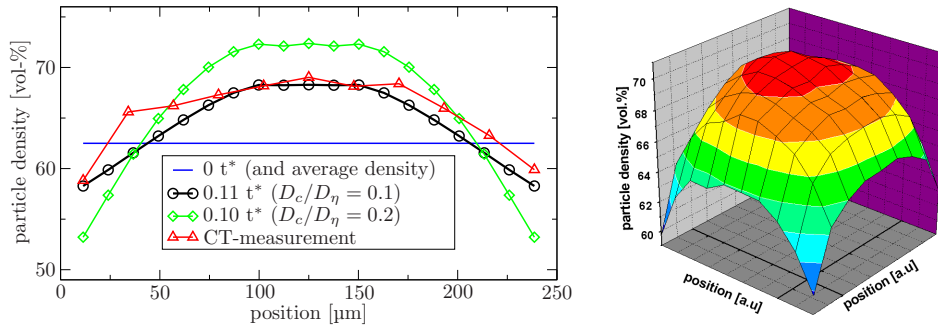


Figure 3. Left: Snapshot of the powder density at the centre line of a quadratic cross-section for $D_c/D_\eta = 0.1, 0.2$. The time is given as multiples of the time unit $t^* \approx 66$ ns. Also shown is our CT-measurement at the centre line. Symbols represent measurement points while lines are for guiding the eye. Note that the average concentration at the centre line increases in time due to a net migration to the centre. Right: 2D-plot of the CT-measurement [9].

particles naturally reproduce the large deformations and the free-surface-dynamics of the feedstock-material which do not have to be extracted from a fixed grid. By the SPH-discretisation of Phillips' model presented in this work, it is now possible to track directly the solid load for which no CT-data are available. This is shown in figs. 4 c) and d) which focus on the gate region. Fig. 4 c) is a snapshot of an early stage of the injection. The distribution of the solid load indicates an aggregation at convex corners (i.e. pointing into the mould material) and a decrease at concave corners. This is intuitively understandable since concave corners are regions of large shear rates. In later stages, the flow close to the gate becomes more homogeneous and directed towards the two arms at the top and the bottom. In these narrow arms strong shear rates occur. The effect can be seen in Fig. 4 d). The concentration in the entrance volume is rather homogeneous and large. Inside the arms the concentration is lower. A larger fraction of the solid particles prefers to stay in the entrance volume where shear rates and flow velocities are lower. Additionally, the solid load has a maximum in the centre of the arms as already observed earlier for flow in a channel.

5. Summary

An SPH-framework was developed which allows to simulate the injection process of MicroPIM. The simulations can be performed in arbitrarily complex 3D geometries.

Shear induced powder migration was incorporated by means of Phillips' diffusive flux model. This model was discretised by formulating a SPH-equation of motion for the occupied volume V_ϕ with exact pairwise conservation properties. The simulations correctly predict powder migration to regions with the lowest shear rates and indicate that, for the available CT-measurements, the measured profile is not a steady state. For injection moulding into complex geometries the simulations predict regions of accumulation of the solids fraction. For a quantitative matching of the transport coefficients D_c and D_η of the Phillips model we suggest CT-measurements for well defined geometries such as long capillaries.

The authors acknowledge funding of this project by the Deutsche Forschungsgemeinschaft (DFG) in the framework of the Sonderforschungsbereich Mikrouformen (SFB499) and by the University of Freiburg through the German excellence initiative.

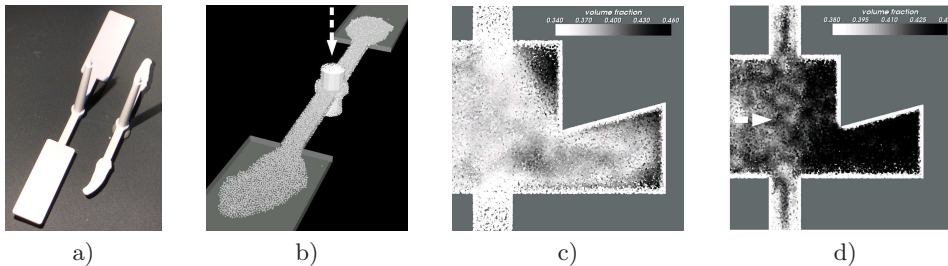


Figure 4. Segregation in a complex geometry. The arrows show the flow direction. a) Parts produced by PIM. b) Snapshot of the simulated filling. c) solid load in an early stage of the mould filling. d) solid load in a later stage.

References

- [1] Baltes, H., Brand, O., Fedder, G. K., Hierold, C., Korvink, J. G., and Tabata, O. (eds.) 2005 *Microengineering of Metals and Ceramics*. Advanced Micro and Nano Systems, Wiley-VCH.
- [2] Bilovol, V. V., Kowalski, L., and Duszczuk, J. 2000 Numerical simulation of the powder injection moulding process for optimization of mould design and process parameters. *Adv. Eng. Mat.*, **2**, 127–131.
- [3] Barriere, T., Gelin, J. C., and Liu, B. 2001 Experimental and numerical investigations on properties and parts produced by MIM. *Powder Metall.*, **44**, 228–234.
- [4] Monaghan, J. J. 2005 Smoothed particle hydrodynamics. *Reports on Progress in Physics*, **68**, 1703–1759.
- [5] Ha, J. and Cleary, P. W. 2005 Simulation of high pressure die filling of a moderately complex industrial object using smoothed particle hydrodynamics. *Int. J. Cast Metals Research*, **18**, 81–92.
- [6] Kauzlarić, D., Lienemann, J., Pastewka, L., Greiner, A., and Korvink, J. G. 2008 Integrated process simulation of primary shaping: multi scale approaches. *Microsys. Technol.*, **14**, 1789–1796.
- [7] Heldele, R., Rath, S., Merz, L., Butzbach, R., Hagelstein, M., and Hausselt, J. 2006 X-ray tomography of powder injection moulded microparts using synchrotron radiation. *Nuclear Instruments and Methods in Physics Research B*, **246**, 211–216.
- [8] Heldele, R., Schulz, M., Kauzlarić, D., Korvink, J. G., and Hausselt, J. 2006 Micro powder injection molding: process characterization and modeling. *Microsys. Technol.*, **12**, 941–946.
- [9] Heldele, R. 2008 *Entwicklung und Charakterisierung von Formmassen für das Mikropulverspritzgießen*. Ph.D. thesis, University of Freiburg.
- [10] Wei, W. C. J., Tsai, S. J., and Hsu, K. C. 1998 Effects of mixing sequence on alumina prepared by injection molding. *J. Europ. Ceramic Society*, **18**, 1445–1451.
- [11] Phillips, R. J., Armstrong, R. C., Brown, R. A., Graham, A. L., and Abbott, J. R. 1992 A constitutive equation for concentrated suspensions that accounts for shear-induced particle migration. *Phys. Fluids A*, **4**, 30–40.
- [12] Krieger, I. M. 1972 Rheology of monodisperse lattices. *Adv. Colloid Interface Sci.*, **3**, 111–136.
- [13] Monaghan, J. J. 1994 Simulating free surface flows with SPH. *J. Comp. Phys.*, **110**, 399–406.
- [14] Cleary, P. W. and Monaghan, J. J. 1999 Conduction modelling using smoothed particle hydrodynamics. *J. Comp. Phys.*, **148**, 227–264.
- [15] Morris, J. P., Fox, P. J., and Zhu, Y. 1997 Modeling low Reynolds number incompressible flows using SPH. *J. Comp. Phys.*, **136**, 214–226.